Available online at www.sciencedirect.com
SCIENCE DIRECT®
Journal of Sound and Vibration 262 (2003) 117–140
JOURNAL OF SOUND AND VIBRATION
www.elsevier.com/locate/jsvi

# Transmission noise identification using two-dimensional dynamic signal analysis

Min-Chun Pan*, Jeng-Xin Chen

*Department of Mechanical Engineering, National Central University, Chung-Li 320, Taiwan, ROC*

Received 20 August 2001; accepted 18 June 2002

**Abstract**

This study aims at identifying transmission noise of two types of electrical vehicles with different transmission systems using the developed two-dimensional dynamic signal analysis (2DSA). Two electrical scooters, more specifically, with a gear transmission system and a continuous variable transmission (CVT) system, respectively, have been taken as test benches due to the whistle-like noise emitting from their transmission systems. To effectively process dynamic signatures measured from rotary machinery with varying speed, and even varying orders during operation, such as a machine with a CVT system or gear-shifting operation, the 2DSA approaches including the order analysis (OA) and the time–frequency analysis have been developed and implemented as processing tools. The specifications of vehicle transmission systems, especially the ratio of each speed reduction, and the tooth (cog, blade, etc.) number of transmission elements, i.e., geometric analysis, are firstly to be examined. After the 2DSA processes the noise measured from test vehicles during wide-open-throttle operation, dominant annoying transmission noise components can be extracted, and their sources can be identified through comparing feature orders obtained from geometric analysis. The procedure can not only identify noise sources but conclude transmission components to be further modified in respect of annoying noise.


## 1. Introduction

Engine-powered vehicles are in general the main source of air pollution in urban regions. Especially, scooters with two-stroke light-cylinder gasoline engines under 100 $cm^3$ have been attributed to the principal mobile source of both air pollutant and environmental noise. Therefore, the work to develop EVs replacing scooters for environmental concerns has become rather urgent recently. For conventional engine-powered vehicles, especially, two-wheel scooters

*Corresponding author. Tel.: +886-3-426-7312; fax: +886-3-425-4501.
*E-mail address:* pan_minc@cc.ncu.edu.tw (M.-C. Pan).

0022-460X/03/$ - see front matter 
doi:10.1016/S0022-460X(02)01024-6

with semi-exposed engines, transmission systems and mufflers, the explosive force knocking on combustion chambers, the crank shaking force/moment on engine units and frame bodies, and the impulses resulting from exhaust flowing in mufflers, contribute to serious noise, vibration and harshness (NVH) problems. Since induction motors associated with pulse-width-modulation inverters instead of engines, with relatively smooth power output, get rid of discharging exhaust, developed and commercialized electrical scooters can mostly cope with concerned air- and noise-pollution problems. On the other hand, the annoying noise emitted from transmission systems becomes especially perceptible without the shielding of intake and exhaust noise. Whistle-like and rattling transmission noise composes the dominant spectral components of EV noise. Many noise-reduction techniques have been explored and developed for decreasing such annoying noise emitted from transmission components, like gears [1–3], power-transmission belts [4–6], chain sets [7–9], and fans for cooling transmission systems [10–11], etc.

All transmission components fall into the category of rotary machinery. Dynamic signals measured from a transmission system correlate to its revolution speed except for resonance regarding signatures. It is often useful to display the amplitude or phase of a frequency spectrum in which the abscissa is scaled according to the r.p.m. of some shaft of interest, so that each harmonic of the shaft rate appears at a fixed point, independent of the shaft speed. This sort of display is called an *order spectrum*, and each harmonic of the shaft speed is called an *order*. Conventionally, two basic methods of order analysis (OA), i.e., the FFT-based method and the resampling-based method [12], have been employed to digitally track orders, which result from rotating components in NVH problems. Recently, a Kalman filtering based method [13,14] has been introduced to track orders, especially for orders with high slew rates, and dynamic signatures of multi-axial systems. In addition, a time-variant discrete Fourier transform scheme [15] has been proposed to offer varying frequency band according to the order of interest.

As a complementary role of the OA, the time–frequency analysis (TFA) can interpret significant events occurring in a single revolution of rotary machinery. In the past two decades, different computation schemes [16–18], besides the spectrogram based on a short-time Fourier transform, have been proposed and implemented in the field of digital signal processing to deal with the issues of time–frequency resolution, interference-term (or ghost-view) severity, and computation efficiency.

Three principal types of transmission system, i.e., the CVT together with speed-reduction gears, the gear sets, and the power-chain sets, have been mostly applied in commercialized electrical scooters. The study selects the former two types as test vehicles to explore transmission noise since the whistle-like and rattling noise forms shrill tones moving in cities and their environs. The dynamic signal analysis (DSA) schemes including the OA and the TFA have been developed and implemented as processing and interpreting tools. To identify the varying order of CVT-belt noise, an adaptive OA based on the geometry of transmission elements has been realized. Additionally, the study illustrates how the geometric analysis can facilitate the task of noise source identification. The dominant annoying spectral components resulting from the CVT-belt and some specific set of gear can be pointed out. This procedure helps conclude guidelines for design modification to reducing annoying transmission noise.

## 2. Theoretical parts

A junction of the OA and the TFA is termed the two-dimensional DSA (2DSA) in this study. In the 2DSA framework, the OA schemes including the FFT-based, the resampling-based and the adaptive geometry-based approach, as well as the TFA schemes consisting of the windowed Fourier transform-based spectrogram, the Wigner–Ville distribution (WVD) and the smoothed WVD (SWVD), have been developed and implemented. Besides, the geometric analysis of a machine can facilitate determining significant annoying frequencies and their trends relative to the running speed of one shaft. Thus, the orders of dynamic signatures relating to a basic revolution speed will be discussed associated with the schematic geometry of transmission components applied in the investigated EVs.

### 2.1. Development of order analysis

#### 2.1.1. FFT-based order analysis

A simple way to characterize significant spectral components relating rotary machine parts is using window Fourier transform (WFT)-based spectrogram, defined as

$$SPE_{Z_f}^{(g)}(t,\omega)=\left|\int_{t''} Z_f(t')g^*(t'-t)\mathrm{e}^{-\mathrm{j}\omega t''}\,\mathrm{d}t'\right|^2, \tag{1}$$

where $Z_f(t)$ is the analytical form of the dynamic signal $f(t)$ measured from rotary machinery, and $g(t)$ the weighting window for each computation. The angular-domain information offered by an encoder or tachometer can subsequently yield revolution speed and compute-related annoying frequency of rotating elements. Therefore, the r.p.m.-frequency spectrum of a dynamic signature can identify the order-related spectral components and their sources.

#### 2.1.2. Resampling-based order analysis

To clearly observe the energy intensity of each order-related spectral component, the r.p.m. order spectrum can be further obtained from the r.p.m.-frequency spectrum via a resampling theorem. The resampling process is to transfer time domain information into the order domain, i.e.,$\Delta t \to \Delta\theta$. The dynamic waveform of equal time increment measured from rotary machinery can be resampled to yield new signature of equal angular increment with the aid of tacho-information. Same as discrete Fourier transform in time domain, the resampled angular-domain data can be transformed into order domain ($\Delta\theta \to \Delta O$) by using the FFT scheme. The following shows an equivalent relationship between the data in the frequency domain and the order domain:

$$f_{sampling}=\frac{1}{\Delta t}\Leftrightarrow O_{sampling}=\frac{1}{\Delta\theta}, \tag{2}$$

$$f_{Nyquist}=f_{\max}=\tfrac{1}{2}f_{sampling}\Leftrightarrow O_{Nyquist}=O_{\max}=\tfrac{1}{2}O_{sampling}, \tag{3}$$

$$\Delta f=\frac{1}{T}=\frac{1}{N\Delta t}\Leftrightarrow \Delta O=\frac{1}{R}=\frac{1}{N\Delta\theta}, \tag{4}$$

where $N$ is the number of total sampled data; $O_{sampling}$ denotes the sampling order, equivalent to $f_{sampling}$ denoting the sampling frequency; and $f_{Nyquist}$ (Nyquist frequency), which is half of the

sampling frequency, represents the maximum frequency, $f_{\max}$, to be analyzed. Likewise, $O_{Nyquist}$ (Nyquist order), which is half of the sampling order, represents the maximum order ($O_{max}$) to be analyzed. In computation, $O_{sampling}$ depends upon $\Delta\theta$ (the sampling degree increment) between each two resampled data, equivalent to $f_{sampling}$ upon $\Delta t$ (the sampling time increment).

### 2.1.3. Adaptive geometry-based order analysis

A dynamic signature measured from the operation of a rotary machine generally consists of resonances and fixed order components, which relate to primary rotating speed of the power source. Additionally, in some machinery with varying order parts, e.g., CVT mechanism and gear shift associated with a planetary gear set, the measured signals include spectral components, whose frequencies are not the fixed multiples of the primary revolution speed. In the study, the geometric relationship of CVT mechanism has been explored for tracking the varying order tune resulting from the CVT operation. Whatever the CVT is in a constant-speed, acceleration, or deceleration condition, it maintains a geometric relationship as sketched in Fig. 1. Equations below illustrate the mathematic relations of those geometric parameters:

$$\tfrac{\pi}{2}(DR_p + DN_p) + 2C\cos\psi + \psi(DN_p - DR_p) = L_p, \tag{5}$$

$$\tfrac{1}{2}(DN_p - DR_p) = C\sin\psi, \tag{6}$$

where $DR_p$ and $DN_p$ are the effective diameters of a driving- and driven-sheave, respectively; $C$ denotes the distance of the driving- and driven-shaft, and $L_p$ the belt length. The value of angle $\psi$ depends upon $DR_p$ and $DN_p$, where $\psi$ is defined as positive if $DR_p < DN_p$. Let $r(t)$ be the speed ratio of the driving sheave to driven sheave, i.e., $r(t) = \omega_1(t)/\omega_2(t) = DN_p/DR_p$, where $\omega_1(t)$ and $\omega_2(t)$ are the instant speed of the driving- and driven-sheave, respectively. Hence, the above geometric relations can be rearranged as

$$\frac{\pi}{2}DR_p(1+r) + 2C\cos\psi + \psi DR_p(r-1) = L_p, \tag{7}$$

$$DR_p(r-1) = 2C\sin\psi. \tag{8}$$

As the revolution speed of the driving- and driven-sheave are measured or indirectly computed, the non-linear equations (Eqs. (7) and (8)) of two independent variants, $DR_p$ and $\psi$, can be numerically evaluated. Finally, the instant CVT-belt revolution speed, $\omega_b$ (in round per second),

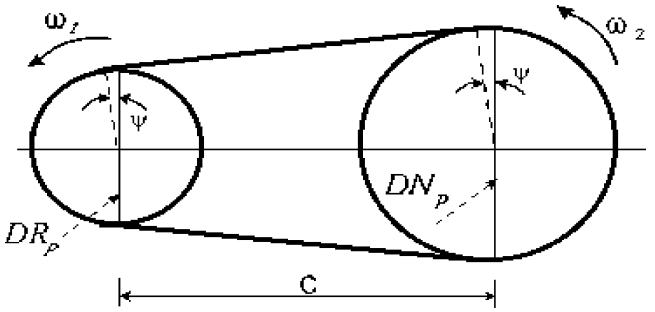


Fig. 1. Schematic diagram of the geometric relationship for a belt (or chain) drive.

with varying order can be obtained, i.e.,

$$\omega_b = \frac{DR_p\omega_1}{2L_p}, \tag{9}$$

or

$$\omega_b = \frac{DN_p\omega_2}{2L_p}.$$

Based on this principle, the geometric and kinematical equations of a transmission system can indicate associated annoying, not only fixed order but also varying order, spectral components of dynamic signals measured during operation.

### 2.2. Development of time–frequency representations

The TFA of a time waveform can be expressed in a generalized form, $C_f(t,\omega;\Phi)$, as shown in Eq. (10), i.e., the so-called Cohen class:

$$C_f(t,\omega;\Phi) = \frac{1}{2\pi}\int\int\int e^{j(\xi t-\tau\omega-\xi u)}\Phi(\xi,\tau)f(u+\tau/2)f^*(u-\tau/2)\,du\,d\tau\,d\xi, \tag{10}$$

where $f(u)$ is the analyzed signal, and $\Phi(\xi,\tau)$ denotes the kernel function to a specific TFA. Derived from the definition of Eq. (10), one can obtain a variant TFA with a specific kernel function.

#### 2.2.1. WFT-based spectrogram

For a non-stationary signal, the Fourier transform of a whole segment of waveform can only reserve spectral information. But the frequency contents at a certain time instant are not available. Sliding weighting window function along the time axis and multiplying time waveform can yield the windowed Fourier transform. Both time and frequency information can thus be obtained. Let $f(t)$ be the analyzed signal, and $g(t)$ the weighting window. If the kernel function $\Phi(\xi,\tau)$ is chosen as the ambiguity function of $g(t)$, i.e.,

$$\Phi_{spect}(\xi,\tau) \equiv \int_{-\infty}^{\infty} g(t+\tau/2)g^*(t-\tau/2)e^{-j\xi t}\,dt, \tag{11}$$

then the WFT-based spectrogram of $f(t)$ can be deduced in the form of Eq. (1). The discrete form of a WFT-based spectrogram can be expressed as

$$SPE_{Z_f}^{(g)}(n,m) = \left|\sum_{k=0}^{M-1} Z_f(k)g^*(k-n)e^{-jmk(2\pi/M)}\right|^2, \tag{12}$$

where $M$ denotes the length of the weighting window $g(t)$; $n$ and $m$ represent the index of discrete time and discrete frequency, respectively. Due to the confinement of the uncertainty principle, one cannot simultaneously obtain both extremely good time and frequency resolution from a WFT-based spectrogram. Some other TFA schemes can cope with this problem.

*2.2.2. Wigner–Ville distribution (WVD)*

When the kernel function equals unity, i.e., $\Phi_{WVD}(\xi,\tau)=1$, the WVD can be yielded [18]:

$$C_f(t,\omega;\Phi_{WVD}) \equiv W_f(t,\omega) = \int \mathrm{e}^{-\mathrm{j}\tau\omega} f(u+\tau/2) f^*(u-\tau/2)\,\mathrm{d}\tau. \tag{13}$$

Substitute Eq. (13) into Eq. (10), the generalized TFA, $C_f(t,\omega;\Phi)$, can be derived to be

$$C_f(t,\omega;\Phi) = \frac{1}{2\pi}\int\!\!\int \phi(t-\tau,\omega-\xi) W_f(\tau,\xi)\,\mathrm{d}\tau\,\mathrm{d}\xi, \tag{14}$$

where $\phi(t,\omega)=\frac{1}{2\pi}\iint \mathrm{e}^{\mathrm{j}(\xi t-\omega\tau)}\Phi(\xi,\tau)\,\mathrm{d}\xi\,\mathrm{d}\tau$. From Eq. (14), it concludes that the generalized form, $C_f(t,\omega;\Phi)$, can be expressed as a 2-D-TF convolution of the WVD of the analyzed signal, and the transformed kernel function, $\phi(t,\omega)$, i.e., imposing FT for $\tau$ and inverse FT (IFT) for$\xi$ upon $\Phi(\xi,\tau)$. To prevent aliasing, the analytical form, $Z_f(t)$, of $f(t)$ has to be applied [19]. Thus, Eq. (13) becomes

$$WV_{Z_f}(t,\omega) = \int_{-\infty}^{\infty} Z_f(t+\tau/2) Z_f^*(t-\tau/2)\mathrm{e}^{-\mathrm{j}\omega\tau}\,\mathrm{d}\tau. \tag{15}$$

The discrete-time form and subsequent implementation procedure of the WVD are given in Ref. [19].

*2.2.3. Smoothed Wigner–Ville distribution (SWVD)*

Eq. (14) indicates that all TFAs can be formulated as a 2D-TF convolution of the WVD of the analyzed signal, and the transferred form, $\phi(t,\omega)$, of a chosen kernel function, $\Phi(\xi,\tau)$. Moreover, if $\phi(t,\omega)$ is a time and frequency decoupled function, i.e., $\phi(t,\omega)=g_1(t)G_2(\omega)\equiv WV_g(t,\omega)$, then the SWVD of the analyzed signal derived from Eq. (14) can be expressed as follows:

$$\hat{SWV}_{Z_f}(t,\omega) = \int\left[\int Z_f\big(t-t'+\tau/2\big) Z_f^*\big(t-t'-\tau/2\big) g_1(t')\,\mathrm{d}t'\right] g_2(\tau)\mathrm{e}^{-\mathrm{j}\omega\tau}\,\mathrm{d}\tau, \tag{16}$$

where $g_2(\tau)$ is the IFT of $G_2(\omega)$ and called the frequency smoothing window, and $g_1(t')$ is called the time smoothing window. If $g_2(\tau)$ is chosen from a real and even function, then we can express

$$g_2(\tau) = \big|\chi\big(\tau/2\big)\big|^2 = \chi\big(\tau/2\big)\chi^*\big(-\tau/2\big).$$

Eq. (16) becomes

$$\hat{SWV}_{Z_f}(t,\omega) = \int\left[\int Z_f\big(t-t'+\tau/2\big) Z_f^*\big(t-t'-\tau/2\big) g_1(t')\,\mathrm{d}t'\right] \chi\big(\tau/2\big)\chi^*\big(-\tau/2\big)\mathrm{e}^{-\mathrm{j}\omega\tau}\,\mathrm{d}\tau. \tag{17}$$

When implementing Eq. (17) in a microcomputer, one can apply an FFT scheme after the computation in the bracket [] has been finished. The evaluation of $\int \bullet \mathrm{d}t'$ in the bracket [], however, is rather time consuming via loop computation. As a matter of fact, the computation of [] in Eq. (17) is exactly $[(Z_f(t+\tau/2)Z_f^*(t-\tau/2))\otimes g_1(t)]|_\tau$, where $\otimes$ denotes convolution integral. In the study, we propose applying and implementing the property of "the convolution in time domain for two signals equivalent to their multiplication in frequency domain then taking IFT". In Section 3, we shall see its efficiency through the comparison of different schemes for computing several synthetic signals.

*2.2.4. Relationship between spectrogram, WVD and SWVD*

When the WVD is evaluated via Eq. (15), it yields interferences between each two mono-components in the TF plane. This makes the interpretation of an analyzed dynamic signal difficult although the WVD offers extremely good TF resolution. On the other hand, the spectrogram via the evaluation of Eq. (12) yields no interferences, but it is confined to the limit of resolution. In the study, we choose $g(t) = (1/\sqrt[4]{2\pi})(1/\sqrt{\sigma_t})e^{(-t^2/4\sigma_t^2)}$ to evaluate the SWVD. Therefore,

$$\hat{SWV}_{Z_f}(t,\omega) = \frac{1}{2\pi}\iint W_g(t-\tau,\omega-\xi)W_{Z_f}(\tau,\xi)\,d\tau\,d\xi. \tag{18}$$

When $\sigma_t\sigma_\omega = \frac{1}{2}$, which satisfies the uncertainty principle, it can be proved that $\hat{SWV}_{Z_f}(t,\omega) = SPE^{(g)}_{Z_f}(t,\omega)$, i.e., the SWVD is identical to the spectrogram with no interferences, but at a sacrifice of resolution [20]. Therefore, one can flexibly tune the value of $\sigma_t$ and $\sigma_\omega$ to obtain different time and frequency resolution. The resulting SWVD yields better TF resolution, especially for $\sigma_t\sigma_\omega < \frac{1}{2}$, but accompanies interferences. It means the illustration of an SWVD with tunable time and frequency resolution, i.e., $\sigma_t$ and $\sigma_\omega$, can go flexibly between the characterization of a spectrogram and a WVD.

## 2.3. Transmission-component-related dynamic signatures

To conduct a geometric analysis for investigating transmission noise emitting from rotary components is inevitable. A rather important phase in any geometric analysis is to count the teeth on every gear, the blades on a cooling fan, and/or the cogs on a V-belt. Speed reduction gears, power transmission belts, and centrifugal fans are especially concerned in the study of vehicle transmission systems. Table 1, a list of rotary-component speeds, incorporates the speeds of the shafts, the expected mesh (or passing) frequencies and various potential "fault-mechanism" (or "annoying-noise" here) frequencies. In the assumed example, the transmission components applied in the test vehicles have been considered:

- shafts—one output and two transfer,
- gear sets—gear mesh and eccentric gears,
- planetary gear trains—gear mesh,
- CVT-belt—belt passing,
- centrifugal fan—blade passing.

Normally, the output shaft is used as a reference since the typical operating speed of this shaft is most frequently known. The relative speeds shown in Table 1 are normalized with respect to the output shaft. It can be noted that a full geometry description is given in the caption of Table 1. To address how the table can be used, "gear sets" is taken as an example. Two frequent dynamic characteristics during operation, i.e., gear mesh and eccentric gears, are considered here. As two transfer shafts are assumed (refer to Fig. 4, counter- and driving-shaft), *two* gear-mesh and *four* eccentric-gear conditions can be expected. They are low-speed and high-speed *gear mesh*, as well as *eccentric* output gear, transfer pinion, transfer gear and driving pinion. In addition, the right column of Table 1 characterizes corresponding dynamic frequencies of all transmission-element conditions in condition of the output shaft with a speed of 1500 r.p.m.

Table 1
A list of normalized rotary-component speeds (equivalent to *order*) based on the final output-shaft from the schematic geometry

| Item | | Normalized frequency (order) based on output-shaft speed | | Operating speed and corresponding dynamic frequency (Hz) | |
|---|---|---|---|---|---|
| *Shafts* | | | | (1500 r.p.m.) | |
| Output | | 1 | | 25 | |
| Transfer[a] | | $R_2$ | $R_1R_2$ | $25R_2$ | $25R_1R_2$ |
| Motor[b] | | $RR_1R_2$ | | $25RR_1R_2$ | |
| *Gear sets* | | | | | |
| Gear meshes | Low-speed (secondary) mesh | $N_{g2}$ (or $R_2N_{p2}$) | | $25N_{g2}$ | |
| | High-speed (primary) mesh | $R_2N_{g2}$ (or $R_1R_2N_{p1}$) | | $25R_2N_{g2}$ | |
| Eccentric gears | Output gear | $N_{g2}\pm1$ | | $25(N_{g2}\pm1)$ | |
| | Transfer pinion | $N_{g2}\pm R_2$ | | $25(N_{g2}\pm R_2)$ | |
| | Transfer gear | $R_2N_{g2}\pm R_2$ | | $25(R_2N_{g2}\pm R_2)$ | |
| | Driving pinion | $R_2N_{g2}\pm R_1R_2$ | | $25(R_2N_{g2}\pm R_1R_2)$ | |
| *Planetary gear train*[c] | | $\left(1+\frac{T_{sun}}{T_{ring}}\right)\bar{R}$ | | $25\left(1+\frac{T_{sun}}{T_{ring}}\right)\bar{R}$ | |
| Gear mesh | | $T_rN_p\left(1+\frac{T_{sun}}{T_{ring}}\right)\bar{R}$ | | $25T_rN_p\left(1+\frac{T_{sun}}{T_{ring}}\right)\bar{R}$ | |
| *CVT-belt*[d] | | $\frac{DN_p\pi}{L_p}\underline{R}$ | | $25\frac{DN_p\pi}{L_p}\underline{R}$ | |
| Belt passing ($N_b$: number of cogs) | | $N_b\frac{DN_p\pi}{L_p}\underline{R}$ | | $25\,N_b\frac{DN_p\pi}{L_p}\underline{R}$ | |
| *Centrifugal fan*[e] | | $R_{total}$ | | $25R_{total}$ | |
| Blade passing | | $N_fR_{total}$ | | $25N_fR_{total}$ | |

[a] Two-stage speed-reduction gear sets assumed, where $R_1$ and $R_2$, respectively, are speed ratios.
[b] Speed ratio, $R$, assumed if other transmission components exist between motor and transfer (gear-set) shafts.
[c] Assume carrier as input, ring-gear as output, and sun-gear fixed, and denote $\bar{R}$ as the speed ratio between ring-gear and the final output shaft.
[d] Speed ratio, $R$, assumed between the back CVT-sheave, and the final output shaft.
[e] The centrifugal fan, which is one part of the front CVT-sheave and mounted on the motor-shaft, the total speed reduction denoted as $R_{total}$.

## 3. Implementation of 2DSA approaches

Before the implemented 2DSA approaches are applied in the analysis of real signals measured from riding vehicles, synthetic signals are firstly designed to assess their effectiveness. By means of this, some theoretical characteristics between different schemes, such as the issue on tracking specific orders using the OA and the issue on the resolution of the TFA, can be compared numerically.

### 3.1. Numerical implementation of order analysis

For the OA, a synthetic signal, whose spectral components are illustrated in Table 2, is composed of resonance, fixed order and varying order signatures, associated with Gaussian white noise. It is assumed the output shaft speeds up to 9000 r.p.m. in 5 s with a constant slew rate of 1800 r.p.m./s, as shown in Fig. 2(a). Besides, the r.p.m. spectrum and order spectrum of the synthetic signal are illustrated in Figs. 2(b) and (c), respectively. In the order spectrum, five vertical lines demonstrate the fixed order components, the linearly order-increasing line denotes the varying order component, and two quadratic curves whose orders decrease as r.p.m. increases are in fact the resonances. This example demonstrates that dynamic signals measured from a rotary machine can be effectively characterized by their order spectra.

### 3.2. Numerical implementation of time–frequency representations

Likewise, four synthetic signals have been designed to verify the validity of different TFA schemes as well as to address their individual characteristics. The purpose is to compare objectively the TF resolution, their individual computation efficiency, and the smearing effects of a TFA caused by interferences. Four signals are described as follows. They are $f_a(t)$: four pieces of short-term sinusoids together with white noise; $f_b(t)$: two impulses appended to a frequency modulation (FM) signal; $f_c(t)$: one impulse appended to two sinusoids; $f_d(t)$: two FM signatures (one with linearly increasing frequency, and the other with linearly decreasing frequency) associated with one impulse and two short-term sinusoids. Fig. 3 illustrates the TFAs of four synthetic signals, where four columns from left to right are the time waveform, the spectrograms, the WVDs, and the SWVDs. Table 3 summarizes the computation CPU time for four synthetic signals with three TFA schemes. Besides, the revised SWVD computation techniques are included

Table 2
Illustration of signature components of the synthetic signal for order analysis (RPM denoted as the basic revolution speed)

| Signature type | Definition of signature components | | | | | | |
|---|---|---|---|---|---|---|---|
| Fixed order signatures | Order | 1 | 2 | 4 | 10 | 20 | |
| | Amplitude | 10 | 10 | 10 | 10 | 10 | |
| Varying order signatures | Order | | | r.p.m./300 | | | |
| | Amplitude | | | 10 | | | |
| Resonance signatures | Frequency (Hz) | | 2000 | | | 4000 | |
| | Amplitude | | 10 | | | 10 | |
| Gaussian white noise | Amplitude | | | 3 (SD) | | | |

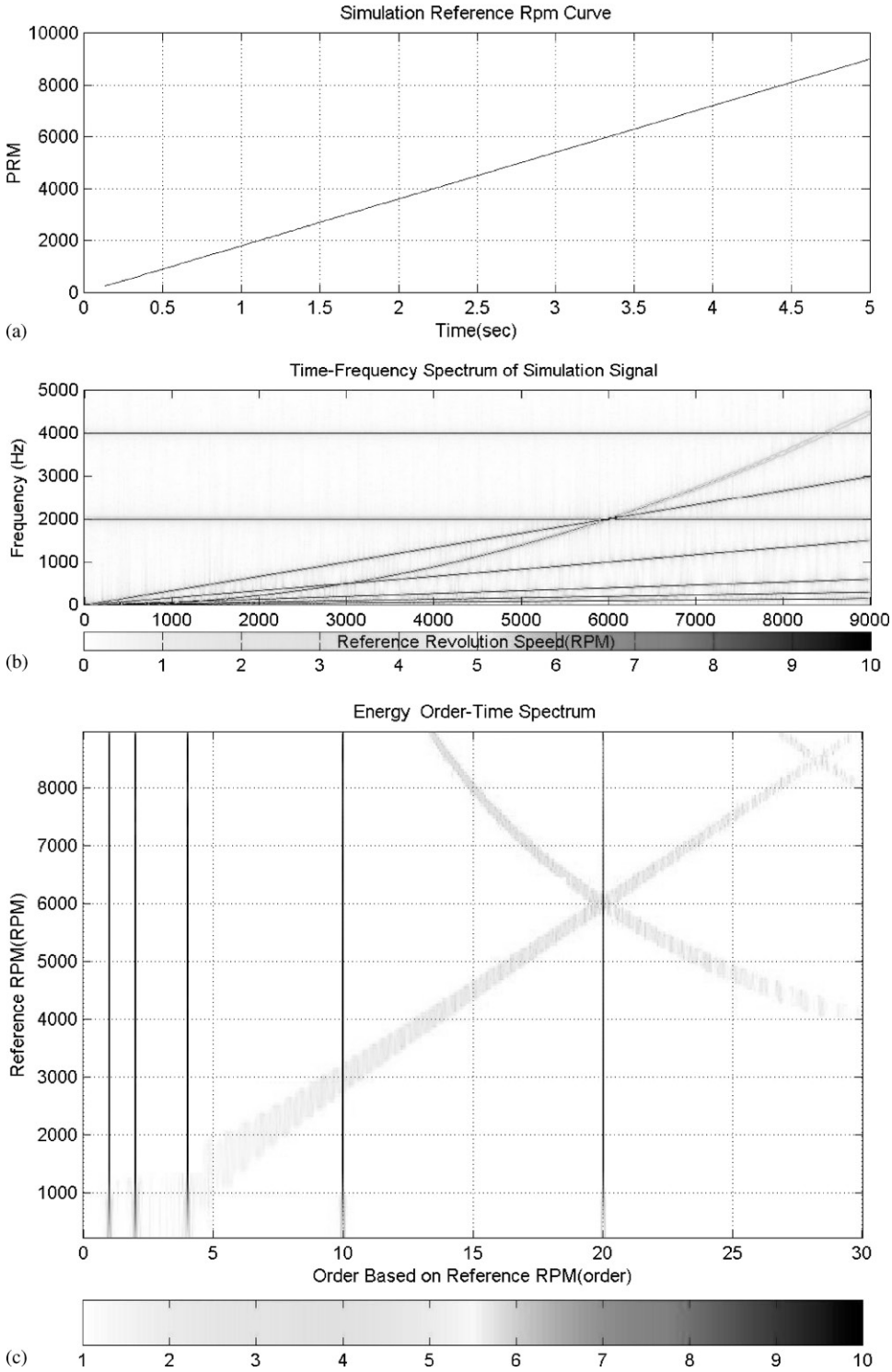


Fig. 2. Order analysis of synthetic signal: (a) Simulated base revolution speed; (b) r.p.m. spectrum of synthetic signal; (c) order spectrum of synthetic signal.

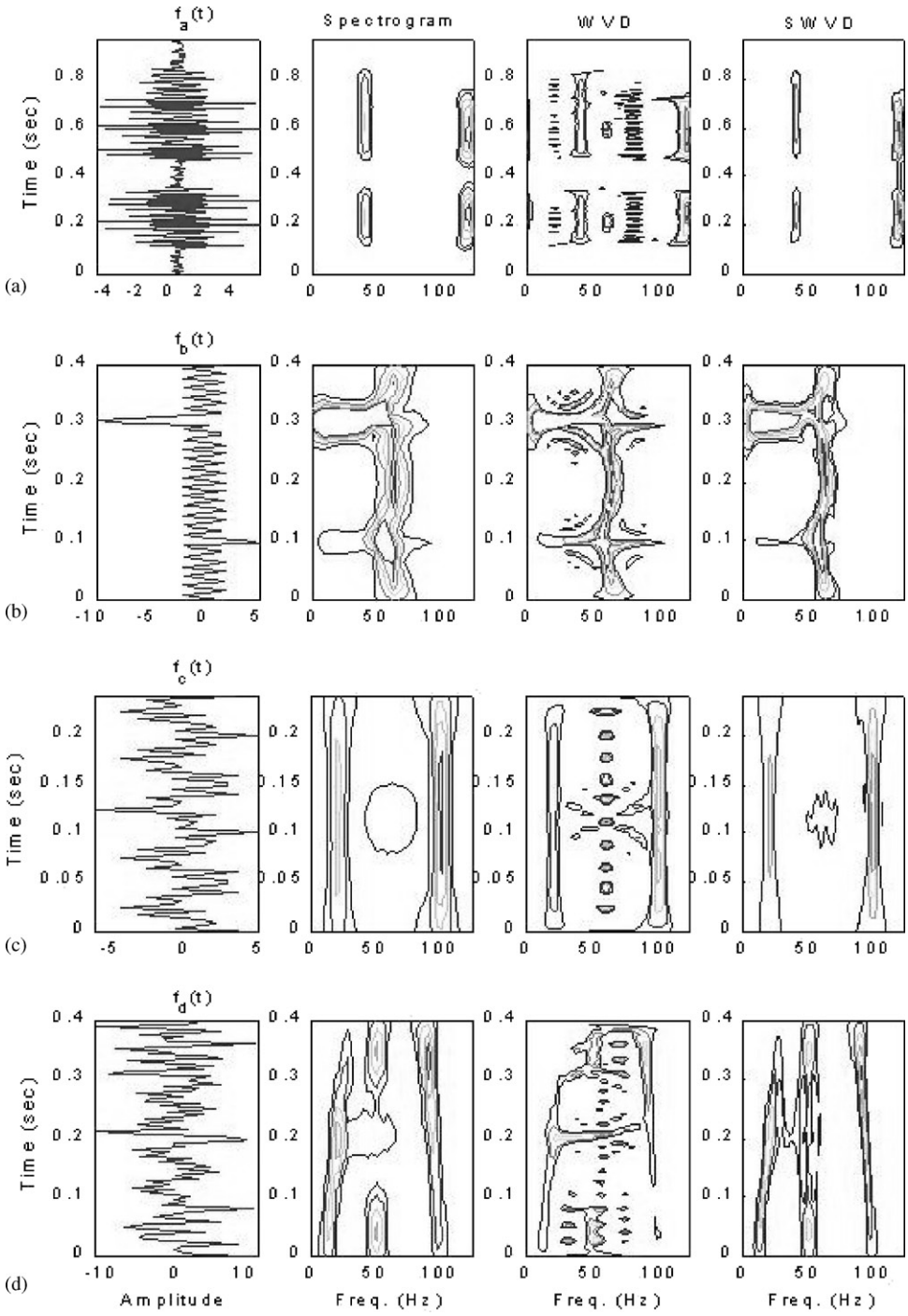


Fig. 3. TFAs of four synthetic signals (the first column: time waveform; the second column: spectrogram; the third column: WVD, and the fourth column: SWVD).

Table 3
Computation CPU time (Pentium II 350) of four synthetic signals with different TFA schemes (CPU times in seconds)

| Synthetic signals | Schemes of TFAs | | | |
|---|---|---|---|---|
| | Spectrogram | WVD | SWVD | |
| | | | *A* | *R* |
| $f_a(t)$ | 0.66 (1) | 1.10 (1.67) | 61.79 (93.6) | 2.8 (4.24) |
| $f_b(t)$ | 0.16 (1) | 0.27 (1.69) | 6.81 (42.6) | 0.6 (3.75) |
| $f_c(t)$ | 0.17 (1) | 0.28 (1.65) | 15.93 (93.7) | 0.77 (4.53) |
| $f_d(t)$ | 0.27 (1) | 0.44 (1.63) | 26.3 (97.4) | 1.26 (4.67) |

In the "SWVD" column, "*A*" denotes original computation scheme, "*R*" denotes applying FFT technique in the computation of convolution integral.

as well. In the analysis, both the spectrogram and the WVD utilize the Gaussian window. To formulate the Gaussian weighting function, $\sigma_t = 0.04$ was set except that $\sigma_t = 0.02$ for the synthetic signal $f_b(t)$. In the computation of the SWVDs, $\sigma_t\sigma_\omega = \frac{1}{4}$ was chosen. This increases the TF resolution of the SWVD up two times as the spectrogram of the same analyzed signal. From the results, some remarks can be made as follows:

- All the three TFA techniques can characterize a dynamic signature in a TF plane to interpret its physical meanings.
- As the WVDs in a format of contour are shown in Fig. 3, the interferences between each two mono-components oscillate in the TF plane with positive and negative values. These terms usually affect correct recognition on significant spectral components.
- Both TF resolution and interferences regard the validity of signature interpretation. The spectrograms offer no interferences but bad TF resolution. The TF resolution of WVDs is extremely good. Interferences, however, appear in between each two mono-components. Compared to the other two TFAs, the SWVDs propose a compromised option between resolution and interference. In numerical evaluation of an SWVD, as $\sigma_t\sigma_\omega = \frac{1}{2}$ is to be set, as identical result to the spectrogram can be yielded.
- The computation efficiency of individual TFA scheme regards its applications. The spectrograms need least CPU time. Based on the time needed for computing spectrograms of four synthetic signals, the WVDs spend around 0.66 times longer, and the SWVDs take tremendous CPU time (90 times more) for original computation scheme. As applying the FFT techniques in the convolution integral of Eq. (17), the time to evaluate an SWVD decreases to 4.5 times that of the spectrogram (see the "*R*" column of Table 3). Moreover, when some numerical procedures are improved, the computation time can be saved further [20].

## 4. Experimentation—investigation on transmission noise

In the study, the annoying noise of two electrical scooters with different types of transmission system is to be investigated. One is using a CVT system and a two-stage speed reduction gear set (one pair of helical gears and spur gears, respectively). The rotary parts of the CVT system include

a speed-varying cog belt and two CVT sheaves, where a forming cooling centrifugal fan is attached to the driving sheave. The other is using a planetary gear system coupled with a centrifugal clutch (i.e., gear-shifting), and a four-stage speed-reduction gear set (two pairs of helical gears, and spur gears, respectively).

### 4.1. Electrical scooter with CVT system

The first test EV with a CVT system emits whistle-like annoying noise during the riding condition. The developed geometry-based OA has been applied in the noise-source identification. In order to decipher what the machine is trying to "say", it is necessary to perform some geometric analysis before embarking on field measurements. A sketch of the transmission system is illustrated in Fig. 4. Based on Table 1 regarding normalized rotary-component speeds, potential transmission noise of interest can be summarized in Table 4. It can be noted that the speed-reduction ratio of CVT mechanism is not a fixed number, which depends upon both the motor speed and road resistance.

The experimentation was conducted at a general-purpose laboratory with a background-noise level of 46 dBA. Since the transmission annoying noise can be clearly perceptible, it is acceptable for comparative experiments regarding noise source identification. Fig. 5 illustrates the measurement set-up. Test conditions during experimentation can be summarized as follows:

- The vehicle runs up with a wide-open-throttle condition till around 7500 r.p.m. of motor-speed (or 900 r.p.m. of rear-wheel speed, equivalently), and then it coasts down with the throttle fully closed.
- The main stand is raised to simulate a no- or low-load condition.
- The noise-pickup microphones are placed at 30 cm high, and 30 cm off the vehicle.
- An accelerometer is mounted on the L-case, which accommodates the speed-reduction gears subsequent to the CVT set, to measure the vibration signals of gear transmission.
- The sampling frequency is 18 kHz, and the anti-aliasing low-pass filter is tuned at 10 kHz.

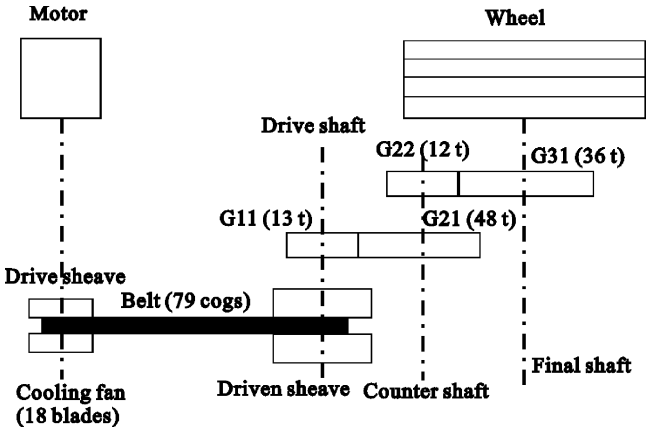


Fig. 4. Schematic diagram of transmission system of the electrical scooter with CVT mechanism.

Table 4
Potential characteristic orders of dynamic signals resulting from transmission elements of the EV with CVT mechanism

| Rotary elements | | Base revolution speed | |
|---|---|---|---|
| | | Normalized by motor speed | Normalized by rear-wheel speed |
| Output shaft of motor | Driving sheave of CVT | 1 | |
| Blade-passing frequency of centrifugal cooling fan (on CVT driving sheave) | | 18 | |
| Motor rotor | | 24 | |
| CVT cog belt | | | $11.1\frac{DN_p\pi}{L_p}$ |
| Passing frequency of CVT cog belt | | | $11.1N_b\frac{DN_p\pi}{L_p}$ $(N_b=29)$ |
| Driven sheave of CVT | Shaft of gear G11 | | 11.1 |
| Meshing frequency of helical gears G11 and G21 | | | 144 |
| Shaft of gears G21 and G22 | | | 3 |
| Meshing frequency of spur gears G22 and G31 | | | 36 |
| Shaft of gear G31 | Rear wheel | | 1 |

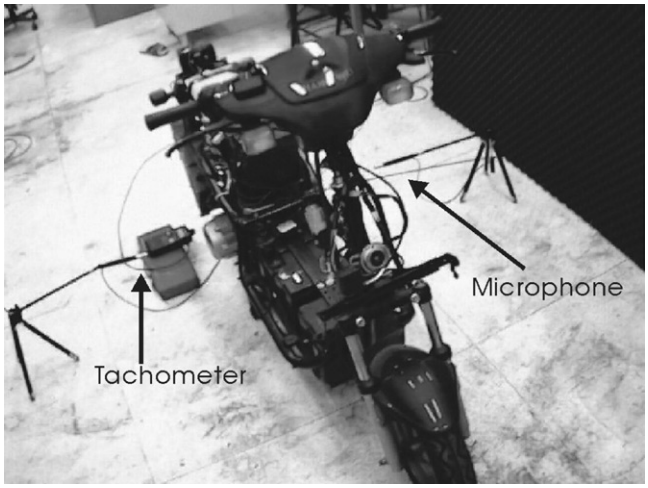


Fig. 5. Measurement setup of electrical scooter with CVT.

- Both the Hall-effect pulse data of the motor, and the photocell pulses from the rear wheel have been acquired to compute their rotating speeds.

The revolution speed (or corresponding *order*) for each rotary component of the transmission system can be computed applying the aforementioned kinematical equations, i.e., the geometric relationship of the CVT mechanism, together with two stages of gear speed reduction. The multiples (i.e., the number of belt-cog, fan-blade, gear-tooth, etc.) of the revolution speeds for the

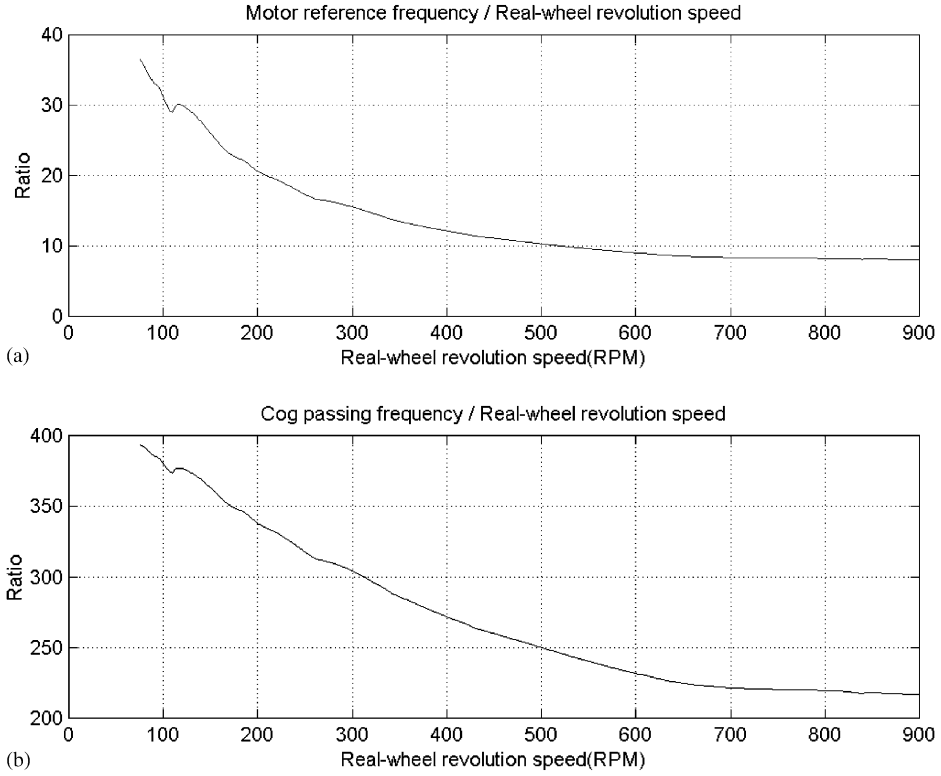


Fig. 6. Speed ratio plot: (a) Motor to rear wheel; (b) cog-passing to rear wheel.

transmission elements usually indicate some probable annoying *orders*, as illustrated in Table 4. Fig. 6 shows the speed ratios of motor and cog passing to the rear wheel, respectively, i.e., the orders based on the rear-wheel speed. It is noted that both the motor speed and cog passing are varying orders resulting from varying speed ratio of the CVT mechanism. An order-spectrum map can characterize different order components with high-energy intensity. From the order spectrum of a measured riding noise based on rear-wheel speed, shown as in Fig. 7(a), varying orders of motor speed and cog passing can be characterized, and the order-144 (meshing frequency of helical gears G11 and G21, referring to Table 4) annoying noise is to be indicated as well. The order-36 component, i.e., the meshing frequency of spur gears G22 and G31, is concluded being not a problem via processing. From the same order spectrum but using another series of number indicated, e.g., 11, 22, 33, and 44, etc., illustrated in Fig. 7(b), the revolution speed and its higher harmonics of the CVT driven sheave contain relatively high sound energy. When the motor speed is chosen as a base revolution speed, the measured noise can be recomputed and its order map is illustrated in Fig. 8. At this instant, only order components resulting from machine parts mounted on the output shaft of the motor remain constant. An order-1 component is illustrated, which characterizes the dynamic signature emitting from the CVT driving sheave (referring to Table 4), different from a varying order demonstrated in Fig. 7(a). Additionally, fan noise becomes perceptible during high-speed phase.

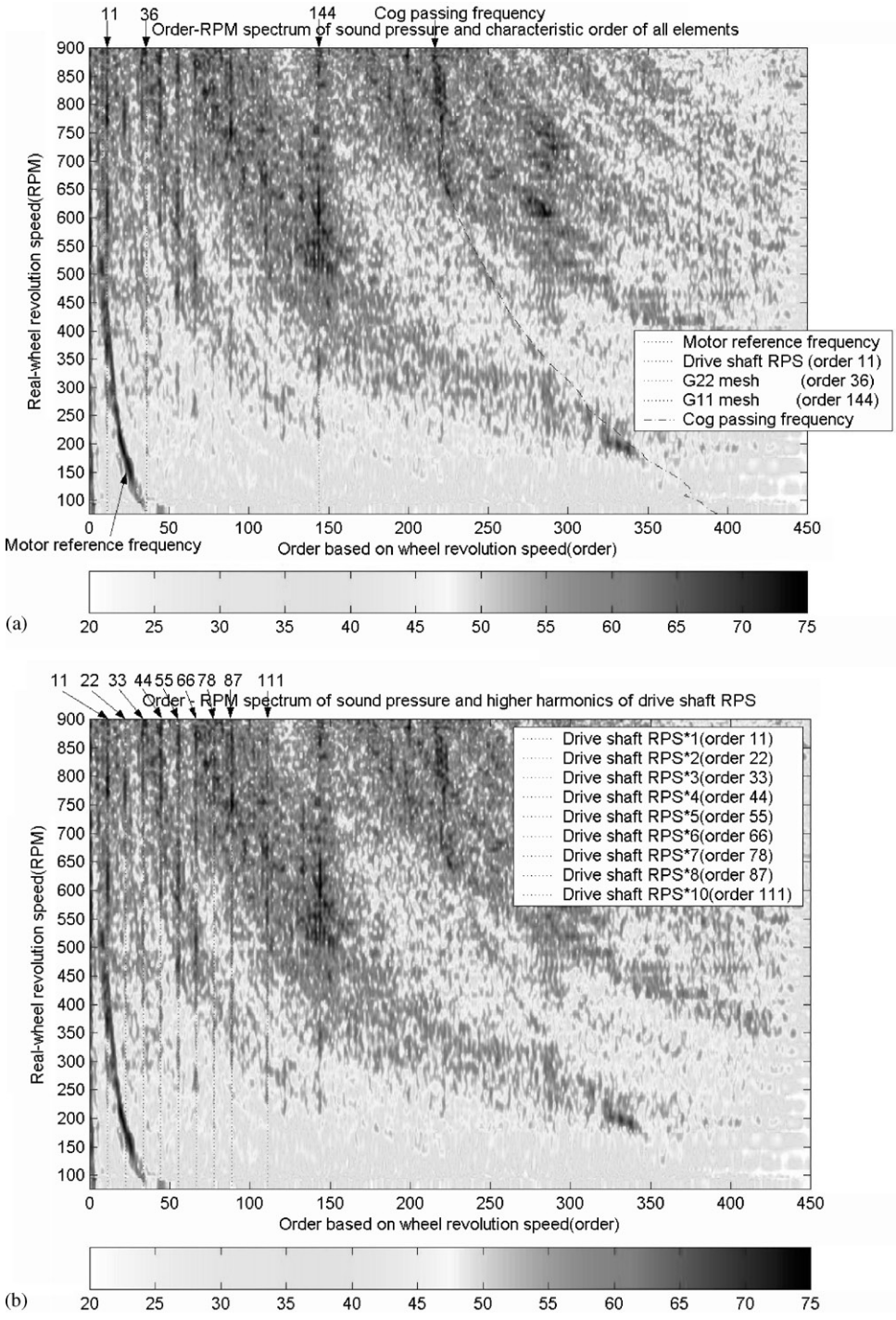


Fig. 7. (Based on rear-wheel speed) Order spectrum of measured EV (with CVT) noise: (a) Passing frequency of CVT-belt, meshing frequency of gears, and rotary frequency of driven CVT sheave are characterized; (b) harmonics of rotary frequency of driven CVT sheave are characterized.

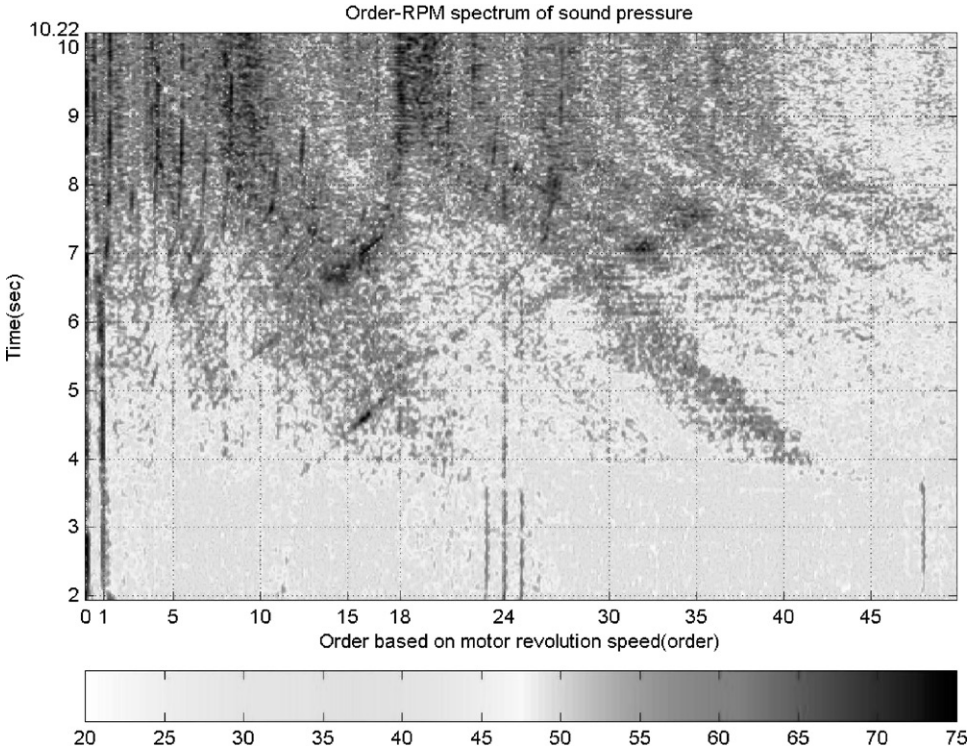


Fig. 8. (Based on rear motor speed) order spectrum of measured EV (with CVT) noise.

Using the 2DSA schemes, the other analysis tool, i.e., the TFA approach, can be applied as well to cope with the problems of phenomenon interpretation and noise-source identification. Fig. 9 shows a TFA illustration with the SWVD using the same riding noise as Figs. 7 and 8. It is noted that the time axis has been replaced by equivalent r.p.m. information. Comparing a TFA plot with characterized curves of different rotating machine parts in rps (r/s, i.e., Hz) along operation time, noise sources can be concluded. Consequently, in Fig. 9, some high-energy spectral components have indicated as to where the sources are from. From the above analysis, some remarks can be concluded below. They also illustrate a proposal of further design modification or manufacturing checks for reducing riding noise:

- Dominant annoying transmission noise includes: (1) rotating noise of CVT driven sheave (order-11 and its higher harmonics, Fig. 7(b)); (2) meshing noise of the G11-G21 gear pair (order-144, Fig. 7(a)); (3) CVT driving-sheave revolution noise during low speed phase (varying order between 36 and 10, Fig. 7; order-1, Fig. 8); (4) CVT-belt noise (varying cog passing order, Fig. 7(a)); and (5) fan noise during high-speed phase (orer-18, Fig. 8).
- Accompanied by the geometric analysis, an order spectrum map can effectively characterize fixed and varying order components. As to resonance-related components that are not changing with revolution speed, to apply TFA is more preferred.

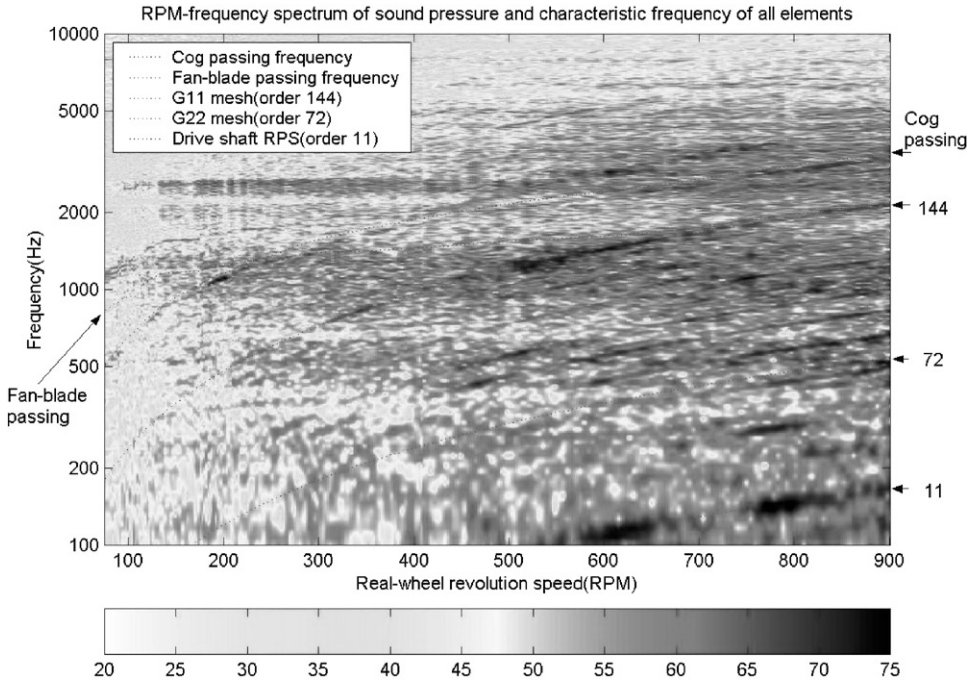


Fig. 9. TFA spectrum of measured EV (with CVT) riding noise, where the time axis is replaced by equivalent rear-wheel speed.

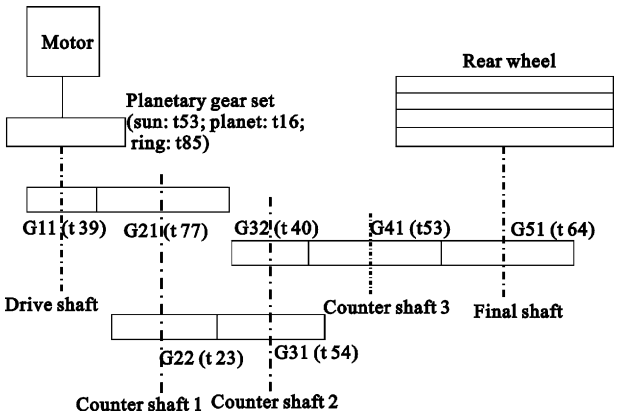


Fig. 10. Schematic diagram of transmission system of the electrical scooter with planetary gear set.

## 4.2. Electrical scooter with gear transmission system

The second test EV with a planetary gear set and four stages of gear reduction also emits annoying riding noise whistling along with the motor speed. A schematic diagram of the transmission system is illustrated in Fig. 10. Table 5 summarizes the characteristic orders of some

Table 5
Potential characteristic orders of dynamic signals resulting from transmission elements of the EV with planetary gear set

| Rotary elements | Probable characteristic orders | Base revolution speed | |
|---|---|---|---|
| | | Normalized by motor speed | Normalized by rear-wheel speed |
| Output shaft of motor | | 1 | |
| Motor rotor | | 24 | |
| Meshing frequency of planet gear and sun gear (valid for high-speed-reduction phase) | | 53 | 638.1 |
| Meshing frequency of planet gear and ring gear (valid for high-speed-reduction phase) | | 32.6 | 393.1 |
| Shaft of gear G51 | Rear wheel | | 1 |
| Meshing frequency of spur gears G51-G41, and G32-G41 | | | 64 |
| Shaft of gear G41 | | | 1.2 |
| Shaft of gears G32 and G31 | | | 1.6 |
| Meshing frequency of helical gears G31-G22 | | | 86.4 |
| Shaft of gears G22 and G21 | | | 3.8 |
| Meshing frequency of helical gears G21-G11 | | | 289.3 |
| Shaft of gear G11 | | | 7.4 |

potential transmission noise as referred to in Table 1. It can be noted that the transmission system maintains a low-speed, $R_{low}$, or high-speed, $R_{high}$, ratio up to the operation of the centrifugal *gear-shifting* clutch, which has been designed and mounted on the planetary gear set:

$$R_{low} = \frac{Motor\_speed\_at\_low\_speed\_phase}{Rear\_wheel\_revolution\_speed} = \left(1 + \frac{G_s}{G_r}\right)\frac{G_{21}}{G_{11}}\frac{G_{31}}{G_{22}}\frac{G_{41}}{G_{32}}\frac{G_{51}}{G_{41}} = 12.04, \tag{19}$$

$$R_{high} = \frac{Motor\_speed\_at\_high\_speed\_phase}{Rear\_wheel\_revolution\_speed} = \frac{G_{21}}{G_{11}}\frac{G_{31}}{G_{22}}\frac{G_{41}}{G_{32}}\frac{G_{51}}{G_{41}} = 7.42. \tag{20}$$

The experimentation has been conducted at the same laboratory as before. In addition, the test conditions used in the former EV are applied again. Fig. 11 illustrates the measurement set-up.

Fig. 12 demonstrates the measured motor and rear-wheel revolution speed, where indicated speed (ratio) phases compose a whole test cycle. From the order spectrum of a measured riding noise based on rear-wheel speed, Fig. 13 illustrates two identical order spectra, but using different indications for better interpretation. Referring to Table 5, it is found that the meshing noise of spur gears G51-G41/G32-G41 (order-64 and its third harmonic, i.e., order-192) is more annoying than that of helical gear pair G21-G11 (order-289) (Fig. 13(a)). As observed from Fig. 13(b), the meshing noise of helical gear pair G31-G22 (order-86 and its higher harmonics) is rather annoying. Additionally, the order component resulting from the revolution of the planetary-gear-set carrier, the same speed as the motor, has been characterized as order-12 (during the low-speed phase, around the rear-wheel speed of 150–250 r.p.m.) and order-7.4 (during the high-speed phase, over the rear-wheel speed of 350 r.p.m.) in Fig. 14. Another clue has been shown in Fig. 13 an order-1 component based on motor speed is characterized.

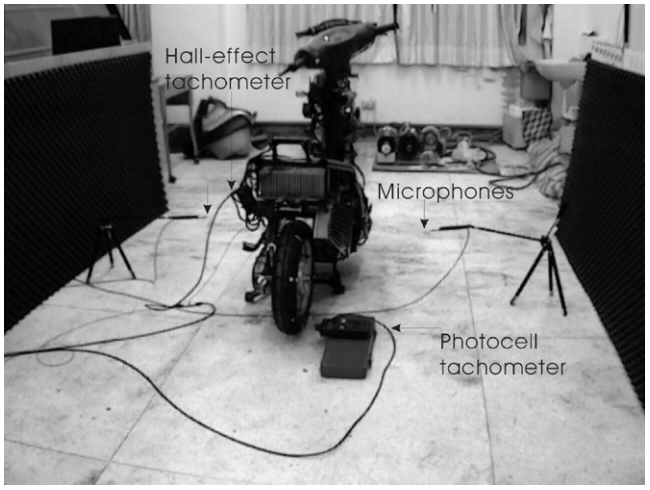


Fig. 11. Measurement set-up of electrical scooter with planetary gear set.

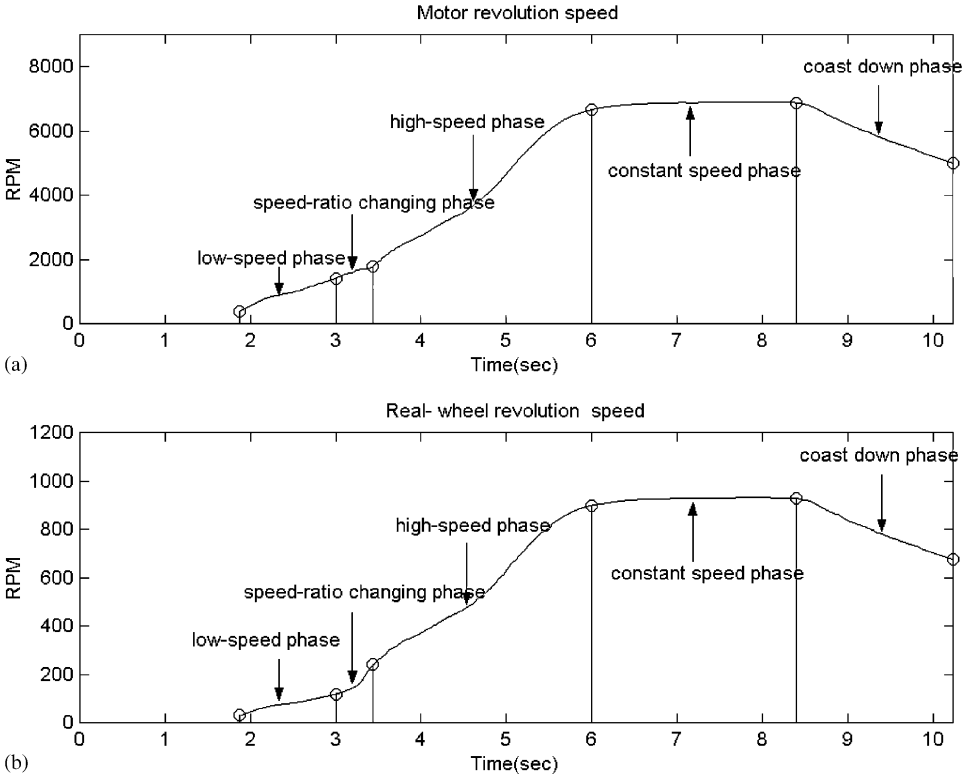


Fig. 12. Revolution speed curves: (a) motor; (b) rear wheel.

To illustrate the TFA being able to cope with this problem as well, Fig. 15 shows the SWVD using the same riding noise as in Figs. 13 and 14. It is noted that the time axis has also been replaced by equivalent r.p.m. information. Some high-energy spectral components have indicated

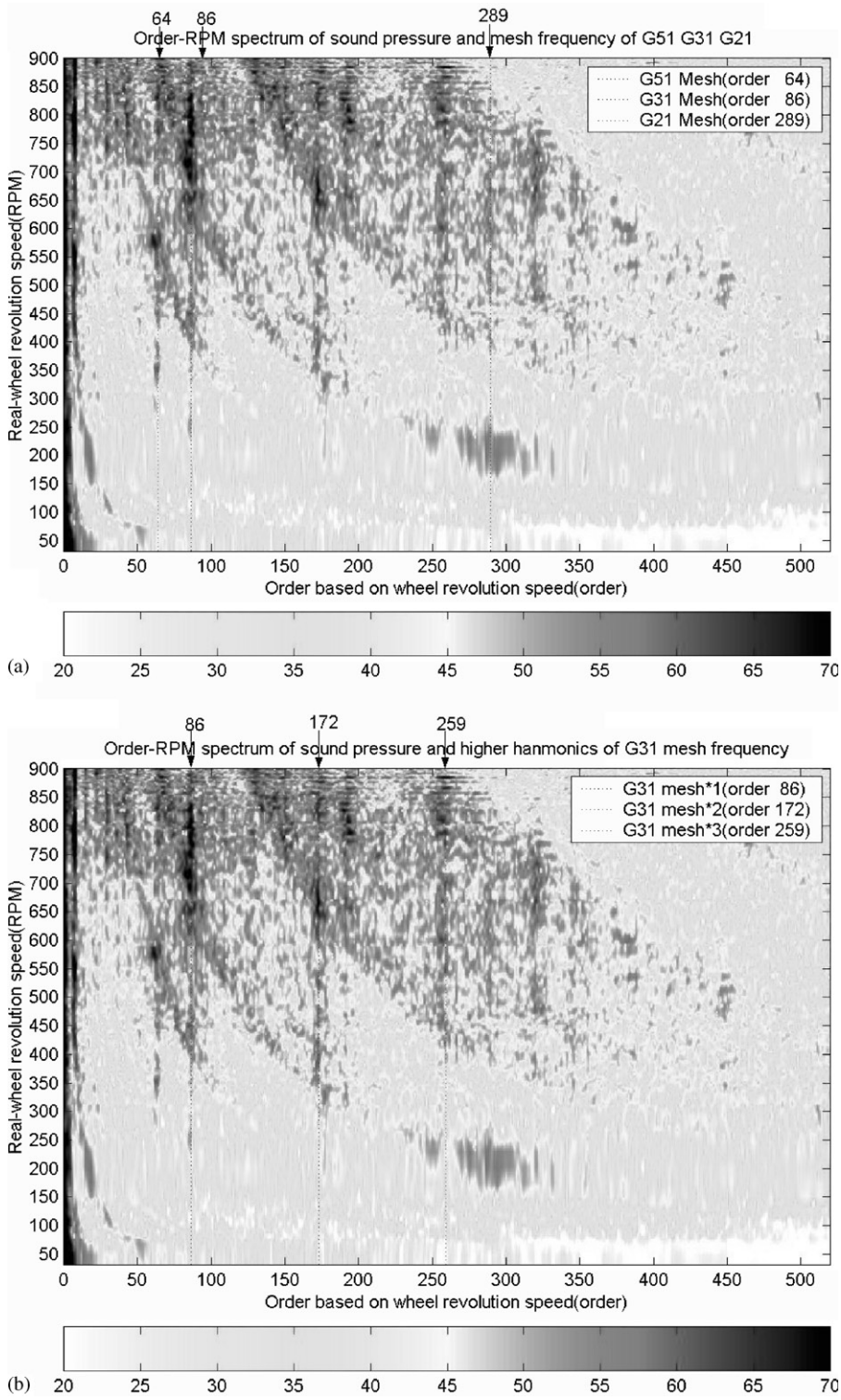


Fig. 13. (Based on rear-wheel speed) order spectrum of measured EV (with planetary gear set) noise: (a) meshing frequencies of gears are characterized; (b) harmonics of meshing frequency of helical gears G22-G31 are characterized.

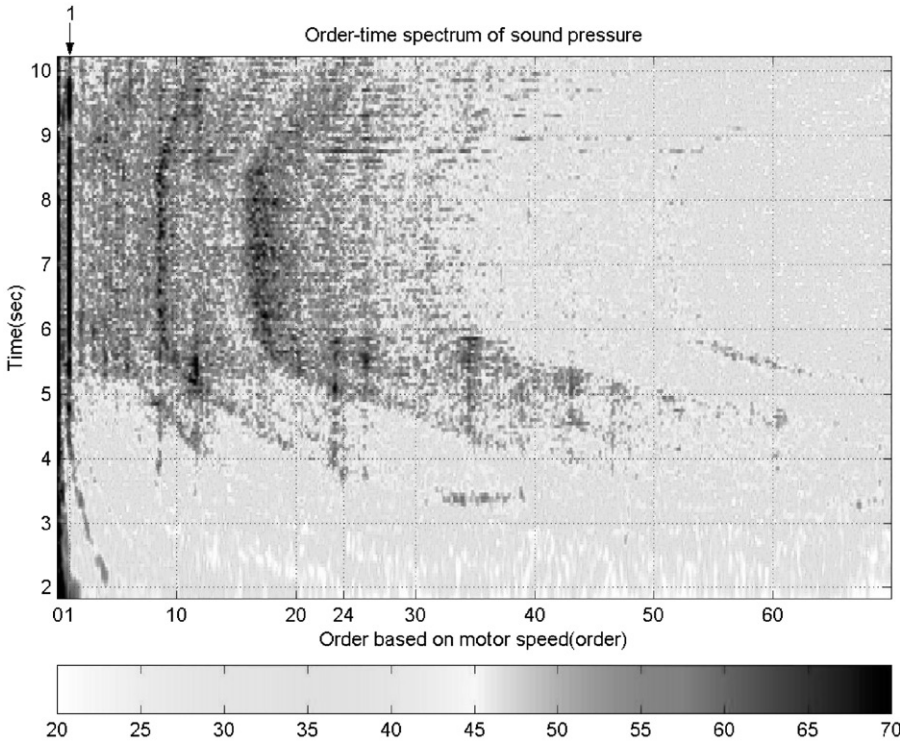


Fig. 14. (Based on motor speed) order map of measured EV (with planetary gear set) noise.

as to where the sources are from. The same results as in the above discussions can be yielded. From the above discussions, some concluding remarks can be made as in the following. Similarly, they can be applied for design and manufacturing rechecks:

- Dominant annoying transmission noise includes: (1) meshing noise of helical gears G31-G22 (order-86 and its higher harmonics, Fig. 13(b)); (2) meshing noise of spur gears G51-G41/G32-G41 (order-64, Fig. 13(a)); (3) annoying noise resulting from the revolution of the planetary-gear-set carrier (orer-1 in Fig. 14).
- The order spectrum map in Fig. 13 can effectively be characterized into two stages of speed reduction of the transmission system, i.e., gear shifting, order-12 at low speed and order-7.4 at high speed.

## 5. Conclusions

In the study, a couple of computation schemes of the 2DSA including the OA and the TFA have been implemented and applied in the transmission noise identification of electrical scooters. Those 2DSA algorithms have been examined and compared via processing various synthetic signals. Two types of the electrical scooters with different transmission systems have been taken to

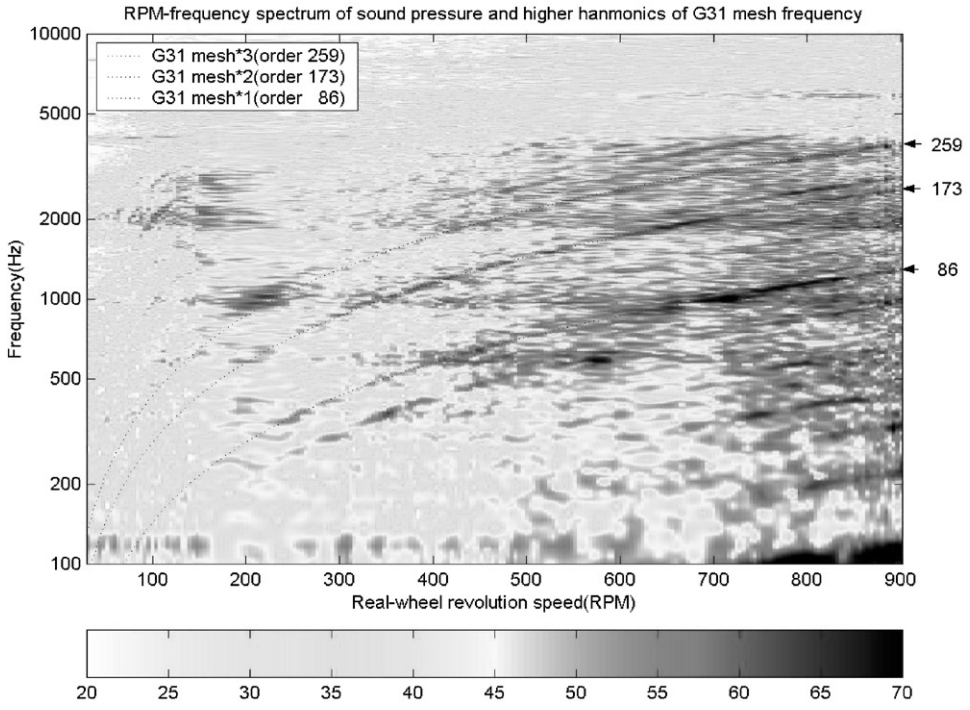


Fig. 15. TFA spectrum of measured EV (with gear transmission system) riding noise, where the time axis is replaced by equivalent rear-wheel speed.

justify the effectiveness of developed schemes. These can be further verified through the geometric analysis of transmission mechanism. Dominant transmission annoying noise can be successfully characterized and identified through the analysis procedure demonstrated in this paper. The purpose of using the 2DSA approaches is two-fold. One is it can rank spectral components affecting sound quality, in addition to identify noise source. The other is the conclusion can be used as a guide of design modification.

## Acknowledgements

This work was partly supported by the National Science Council of the Republic of China under grant NSC-89-2212-E-008-025, which is gratefully acknowledged.

## References

[1] A.N.J. Van Roosmalen, Noise generation mechanism of gear transmissions, Institute of Mechanical Engineers C492/002 (1995) 141–151.

[2] G.W. Blankenship, R. Singh, New rating indices for gear noise based upon vibro-acoustic measurements, Noise Control Engineering Journal 2 (1992) 81–92.

[3] R.G. DeJong, J.E. Manning, Gear noise analysis using modern signal processing and numerical modeling techniques, SAE Paper no. 840478, 1984.
[4] M. Pan, W. Lu, T. Shieh, CVT belt noise of scooters, International Journal of Vehicle Design 30 (3) (2002) 238–250.
[5] H.J. Kaiser, J. Querengasser, G.M. Bundgens, Special noise problems in automotive timing belts, SAE Paper no. 931316, 1993.
[6] K. Wantanabe, T. Koyama, K. Nagai, M. Kagotani, A study on timing belt noise (theoretical analysis for forced transverse vibration of timing belt with parametric excitation), Transactions of the American Society of Mechanical Engineers, Journal of Mechanical Design 112 (1990) 424–429.
[7] M. Pan, T. Shieh, Design modification for reducing silent chain annoying noise, Transactions of ASME, Journal of Mechanical Design 124 (4) (2002) 822–827.
[8] P. Mott, B. Martin, Phased chain system quietly transmits power, Automotive Engineering 103 (12) (1995) 35–41.
[9] K.W. Wang, S.P. Liu, On the noise and vibration of chain drive systems, The Shock and Vibration Digest 23 (7) (1991) 8–13.
[10] W. Neise, Review of noise reduction method for centrifugal fans, Transactions of American Society of Mechanical Engineers, Journal of Engineering for Industry 104 (1982) 151–161.
[11] W. Neise, B. Stahl, Noise reduction in centrifugal fans: a literature survey, Journal of Sound and Vibration 45 (1976) 375–403.
[12] D.K. Bandhopadhyay, D. Griffiths, Methods for analyzing order spectra, SAE Paper no. 840478, 1995.
[13] H. Vold, M. Mains, J. Blough, Theoretical foundations for high performance order tracking with the Vold–Kalman tracking filter, SAE Paper no. 972007, 1997.
[14] H. Vold, J. Deel, Vold–Kalman order tracking: new methods for vehicle sound quality and drive-train NVH application, SAE Paper no. 972033, 1997.
[15] J.R. Blough, D. Brown, H. Vold, The time variant discrete Fourier transform as an order tracking method, SAE Paper no. 972006, 1997.
[16] S. Qian, D. Chen, Joint time–frequency analysis, IEEE Signal Processing Magazine 16 (2) (1999) 52–80.
[17] F. Hlawatsch, G.F. Boudreaux-Bartels, Linear and quadratic time–frequency signal representation, IEEE Signal Processing Magazine 9 (2) (1992) 21–67.
[18] L. Cohen, Time–frequency distributions: a review, Proceedings of the IEEE 77 (7) (1989) 941–981.
[19] B. Boashash, P.J. Black, An efficient real time implementation of the Wigner–Ville distribution, IEEE Transactions on Acoustics, Speech, and Signal Processing 35 (11) (1987) 1611–1618.
[20] M.-C. Pan, Mechanical noise identification using time–frequency representations, in American Society Mechanical Engineers International, DETC 2001, Proceedings of the 18th Biennial Conference on Mechanical Vibration and Noise, DETC2001/V1B21005, 2001.